ISSN 0036-0236, Russian Journal of Inorganic Chemistry, 2021, Vol. 66, No. 2, pp. 163–169. © Pleiades Publishing, Ltd., 2021.
Russian Text © The Author(s), 2021, published in Zhurnal Neorganicheskoi Khimii, 2021, Vol. 66, No. 2, pp. 160–167.

SYNTHESIS AND PROPERTIES OF INORGANIC COMPOUNDS

Role of Hydroxide Precipitation Conditions in the Formation of Nanocrystalline $BiFeO_3$

O. V. Proskurina[a], *, A. N. Sokolova[a], A. A. Sirotkin[a], R. Sh. Abiev[a], and V. V. Gusarov[a]

[a] *Ioffe Physico-Technical Institute, St. Petersburg, 194021 Russia*

**e-mail: proskurinaov@mail.ru*

Received July 18, 2020; revised August 14, 2020; accepted August 27, 2020

Abstract—Nanocrystalline bismuth orthoferrite ($BiFeO_3$) was prepared by soft chemistry. The hydroxide coprecipitation method was shown to influence the formation of nanocrystalline bismuth orthoferrite. Synthetic conditions were determined to prepare nanocrystalline $BiFeO_3$ free of other phases of the Bi_2O_3–Fe_2O_3 system with a narrow crystallite-size distribution and the smallest crystallite size of about 6–7 nm.

Keywords: bismuth orthoferrite, nanocrystals, microreactor, ultrasonic treatment

DOI: 10.1134/S0036023621020157

INTRODUCTION

Considerable interest of researchers in materials based on bismuth orthoferrite ($BiFeO_3$) is due to its unique properties. Bismuth orthoferrite is a room-temperature multiferroic, with a high thermal stability of magnetically ordered and ferroelectric states; its Néel temperature $T_N = 370$°C and Curie temperature $T_C = 830$°C [1]. Bismuth orthoferrite is a semiconductor with a bandgap in the visible light range from 2.1 to 2.8 eV, which allows it to be used as a photocatalyst [2, 3]. It was also proposed to use $BiFeO_3$-based materials in nonvolatile memory devices, piezoelectric devices, sensors, spintronics, etc. [4–7].

The practical use of this promising multi-purpose material is, however, hampered by two main obstacles: firstly, by the complexity of the synthesis of the $BiFeO_3$ phase free of impurities of other phases of the Bi_2O_3–Fe_2O_3 system [8–10], and secondly, the presence of a cycloidal magnetic structure with a period of ~62 nm [11]. The magnetic cycloid causes a significant compensation of magnetic moments, which leads to a weakening of ferromagnetism and a decrease in magnetoelectric coupling. Methods for tuning the magnetic properties of bismuth ferrite-based crystalline materials are doping the structure with impurity components, producing mechanically stressed epitaxial layers, and producing nanopowders with a certain crystallite size [12–16].

The appearance of impurity phases was explained by various reasons: the high volatility of bismuth, nonstoichiometry and changes in the homogeneity region at high temperatures, higher thermodynamic stability of phases coexisting in the Bi_2O_3–Fe_2O_3 system compared to $BiFeO_3$, and the existence of a $BiFeO_3$ eutectoid decay region [8–10, 17].

The difficulty of preparing single-phase bismuth ferrite with a certain crystallite size initiated studies into the formation mechanisms of bismuth orthoferrite under various synthetic conditions [8, 18–23].

The above-listed challenges of preparing bismuth orthoferrite-based materials led to the search for new methods for preparing bismuth ferrite and for improving the already developed methods. Bismuth orthoferrite can be prepared by solid-phase reactions [8, 18, 24], solution combustion synthesis [21, 25–27], soft chemistry [19, 20, 22, 28–31], and ultrasonic spray pyrolysis [32]. Solid-phase synthesis involving high-temperature heat treatment of reagents often yields foreign phases, such as $Bi_{25}FeO_{39}$ and $Bi_2Fe_4O_9$ [8–10]. In addition, solid-phase synthesis does not provide nanosized $BiFeO_3$ particles, while in most cases it is nanocrystalline materials that show significantly better properties compared to micron-sized powders [2, 15, 16, 33].

A well-known advantage of soft chemistry is its potential for providing nanocrystalline materials [34]. At the same time, as a rule, the synthesis of a single-phase product, even though by soft chemistry, requires the increased temperature and process time, while the obtainability of nanocrystalline particles is based on lowering temperature and shortening the formation time [35]. This inconsistency in the synthesis conditions poses the problem of finding methods for intensifying phase formation in order to optimize the formation of nanocrystalline $BiFeO_3$.

The methods used to intensify the chemical reactions of bismuth orthoferrite formation without a sig-

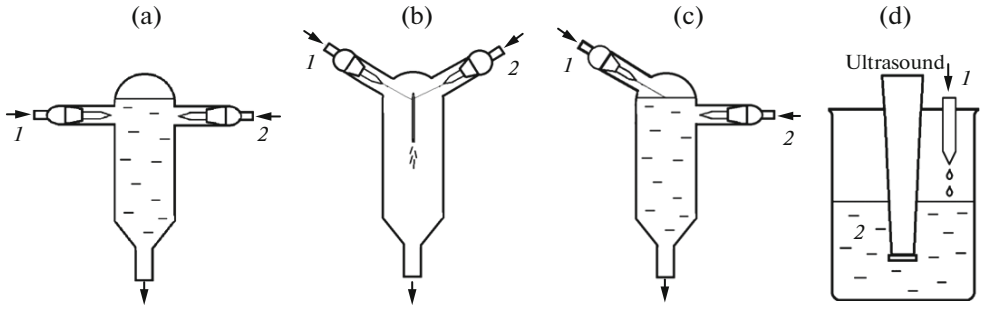

Fig. 1. Schematics of setups used for precipitating hydroxides by (a) method (1), (b) method (2), (c) method (3), and (d) method (4): (*1*) a salt solution mixture and (*2*) a precipitator solution (NaOH).

nificant increase in temperature are such as ultrasonic treatment [36], microwave-assisted hydrothermal synthesis [20, 30], and mechanochemical exposure [37]. Heat treatment of hydroxides coprecipitated in microreactors with free impinging jets has recently been used to prepare nanocrystalline $BiFeO_3$ [23, 31].

The goal of this work is to determine the impact of coprecipitation conditions and heat treatment of coprecipitated hydroxides on the preparation of single-phase nanocrystalline bismuth ferrite with the smallest crystallite sizes.

EXPERIMENTAL

$BiFeO_3$ Synthesis

Nanocrystalline $BiFeO_3$ was prepared by the coprecipitation of hydroxides followed by their heat treatment. The coprecipitation was implemented in four variants: (1) in the submerged-jets mode of the microreactor technique [38]; (2) in the reagent solutions mixing mode in a free impinging-jets microreactor to form the so-called liquid sheet in accordance with the procedure described in [23, 31]; (3) in the reverse precipitation mode with the salt solution mixture fed as a microjet into a precipitator solution through its unconfined surface; and (4) in the reverse precipitation mode with simultaneous ultrasonic exposure. Schematics of setups suitable for these variant methods are shown in Fig. 1.

The initial reagents used were $Bi(NO_3)_3 \cdot 5H_2O$, $Fe(NO_3)_3 \cdot 9H_2O$, 6 M HNO_3, and 4 M NaOH. All reagents were of pure for analysis grade. First, a $Bi(NO_3)_3 \cdot 5H_2O$ weight was dissolved in 6 M HNO_3 for 20 min under magnetic stirring and heating to 70°C; then, the thus-prepared solution was added with $Fe(NO_3)_3 \cdot 9H_2O$ and stirred for another 10 min, after which distilled water was added and stirring lasted another 20 min. The 4 M NaOH was prepared separately. The thus-prepared solutions were used for preparing a mixture of bismuth and iron hydroxides.

For preparing sample **1**, the reactor was filled with NaOH to the level as shown in the scheme (Fig. 1a), which was maintained by means of a hydraulic seal. Then, the nitrate solution and aqueous alkali were simultaneously supplied by Heidolph Pumpdrive 5201 peristaltic pumps through two nozzles, which were arranged on the opposite walls of the reactor at an angle of 180° to each other. One nozzle, 515 μm in diameter, was used to supply the bismuth and iron nitrate solutions; the other nozzle, 470 μm in diameter, to supply NaOH solution. The flow rate of both solutions was 150 mL/min. The jet speed at the nozzle outlet was 15.3 m/s for the mixed salt solution and 16.7 m/s for the aqueous alkali. When the pumps were started, the nitrate solution was "injected" into the reactor filled with NaOH, and the precipitation of metal hydroxides began immediately (Fig. 2). The coprecipitated hydroxide particles formed during the chemical reaction were removed through the hydraulic seal hose to the receiving tank.

For preparing sample **2**, the bismuth and iron salt solutions and the NaOH solution were fed, each at a flow rate of 150 mL/min, through nozzles arranged at an angle of 150° to each other, as free impinging jets to form liquid shroud as shown in Fig. 3. The optimal parameters for reagent supply to a free impinging-jets microreactor (flow rates and the angle between the impinging jets) can be found in [23, 31, 39].

For preparing sample **3**, reverse precipitation was carried out according to the scheme shown in Fig. 1c. The nitrate solution was fed at an angle of 30° to the surface of the alkali solution. At the same time, in order to maintain a constant pH in the mixture, the alkali solution was continuously supplied at the flow rate equal to the flow rate of the bismuth and iron salt solution (150 mL/min).

For preparing sample **4** by reverse precipitation, the nitrate and alkali solutions were mixed under simultaneous exposure to the ultrasound (an I100-6/1 ultrasonic disperser (INLAB), 23 kHz). The mixing lasted 1 min (Fig. 1d).

The hydroxides coprecipitated in four ways were washed with distilled water by decantation to a neutral test and then dried at 65°C for 12 h.

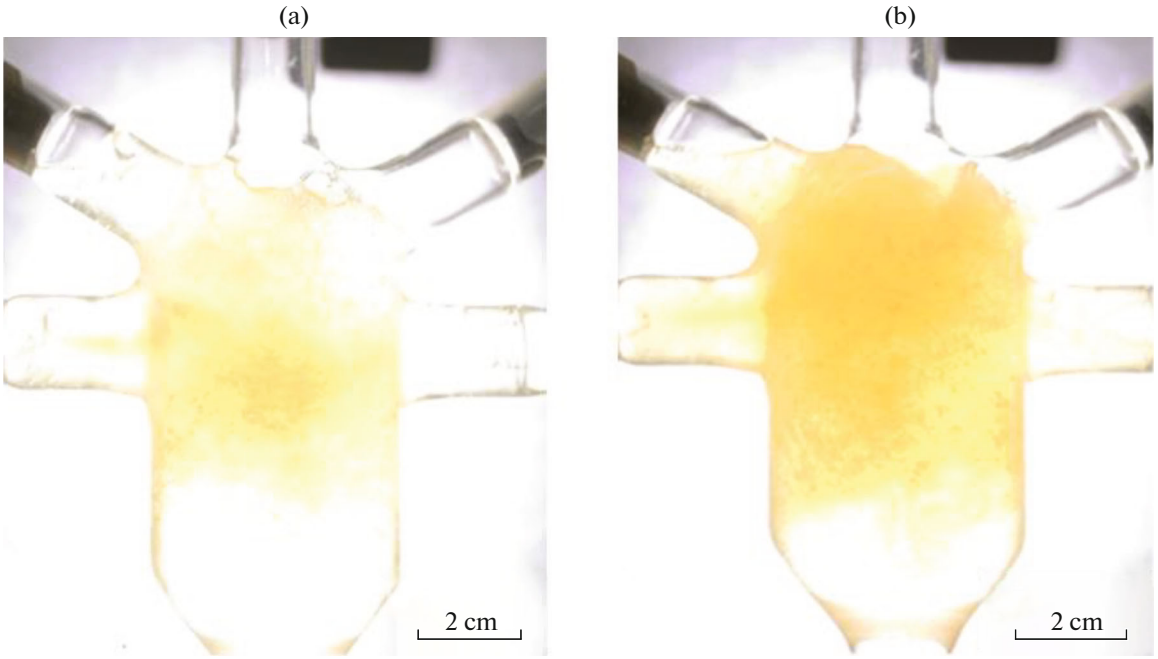

Fig. 2. Microreactor photographed in (a) 0.2 s and (b) 0.4 s after the starting moment of submerged jets mixing in the synthesis of sample **1**.

The heat treatment of samples was carried out as follows. A sample weighing ~30 mg was placed in a platinum crucible that had been warmed in a furnace to stay therein for 4–6 s, after which the crucible was placed in a furnace heated to a certain temperature to stay therein for 30 s, then the crucible was removed and the sample was poured onto a cold metal sheet.

Characterization of Synthesis Products

X-ray diffraction patterns were recorded on a Rigaku SmartLab 3 diffractometer (CoK_α radiation) in the 2θ range from 15° to 72° in 0.01° steps; the counter speed was 0.4 deg./min. Phase analysis was with reference to the database ICSD PDF-2. Crystallite-size distribution and distribution parameters were determined by the fundamental parameters method in the approximation of spherical crystallites and lognormal distribution model using the SmartLab Studio II program package for reflection (012).

Scanning electron microscopy (SEM) experiments and X-ray microanalysis were carried out using a Tescan Vega 3 SBH electron microscope equipped with an Oxford Instruments X-MAX detector.

Transmission electron microscopy (TEM) experiments were performed using a JEOL JEM-2100F microscope with an accelerating voltage of 200 kV. Test sample preparation included dispersing the initial powder in ethanol in an ultrasonic bath for 15 min and subsequent setting on a supporting film.

RESULTS AND DISCUSSION

The results of SEM studies (Fig. 4) showed that in all cases the as-coprecipitated mixture of bismuth and iron hydroxides is represented by agglomerates of par-

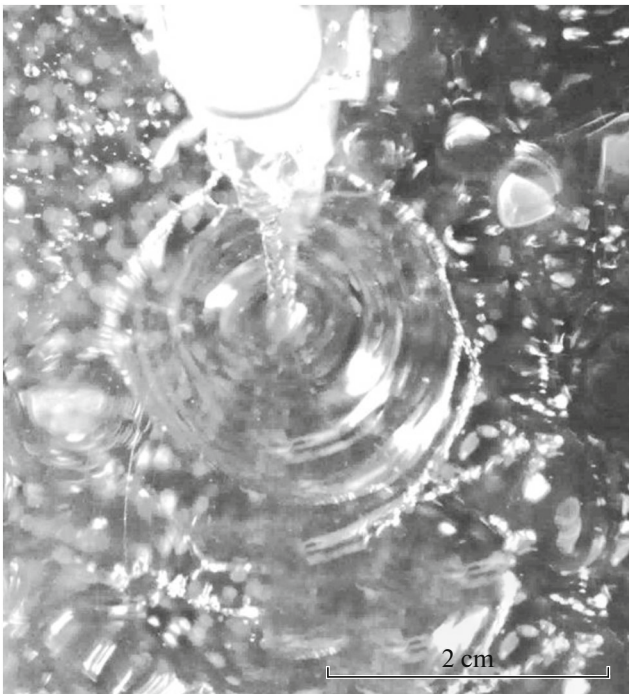

Fig. 3. Liquid sheet photographed in the preparation of sample **2**. The photograph shows the sheet in a plane parallel to the plane of the sheet.

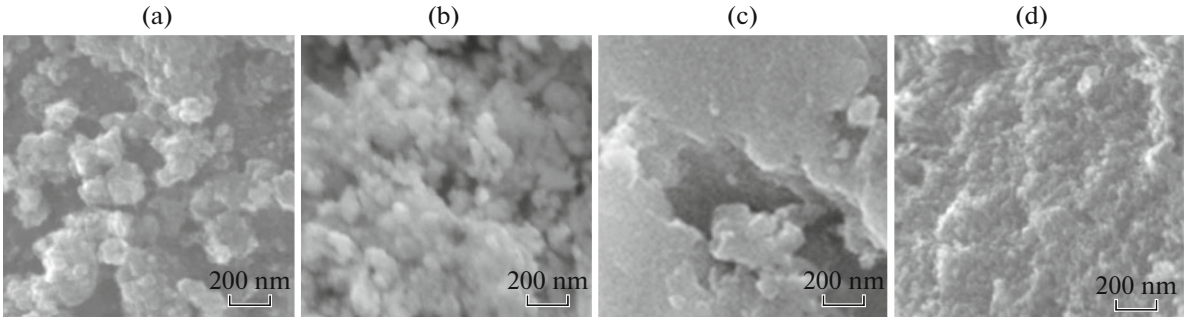

Fig. 4. SEM micrographs of (a) sample **1**, (b) sample **2**, (c) sample **3**, and sample **4** before heat treatment.

ticles. The particle size in all samples varies mainly in the range of 1020 nm. This is also clearly seen in TEM data (Fig. 5). Moreover, the results of electron diffraction and X-ray diffraction analysis show that all as-precipitated samples are represented by an amorphous phase.

In all samples the Bi : Fe atomic ratio as determined by elemental analysis before and after heat treatment remains at the level Bi : Fe = (51 ± 2) : (49 ± 2) at %; within the error bar of the method, this corresponds to the as-batch ratio corresponding to the $BiFeO_3$ stoichiometry.

Figure 6 shows X-ray diffraction data for samples after subsequent heating at 490°C for 30 s (samples **1**–**4**). Almost all reflections in the X-ray diffraction patterns belong to the bismuth orthoferrite phase (Fig. 6). The heat-treatment temperature was chosen to be 490°C for the reason that bismuth orthoferrite formation at this temperature was observed in all samples. Coprecipitated hydroxide samples remain X-ray amorphous before the onset of $BiFeO_3$ formation (at lower temperatures) or when the heat-treatment time is shortened to 20 s, so their X-ray powder diffraction patterns are not shown.

Noteworthy, the $BiFeO_3$ onset crystallization temperature correlates with the end dehydration temperature of the coprecipitated hydroxides, as we can infer from a comparison of the results with simultaneous thermal analysis data [23].

Thus, in this case bismuth orthoferrite formation can be represented as a sequence of the following transformations at increasing temperature:

$$am\text{-}(Bi_2O_3, Fe_2O_3)\cdot nH_2O \xrightarrow{-H_2O,\ T\sim 400\text{–}450^\circ C,\ \tau_1} am\text{-}(Bi_2O_3, Fe_2O_3) \xrightarrow{T\sim 490^\circ C,\tau_2} BiFeO_3, \quad (1)$$

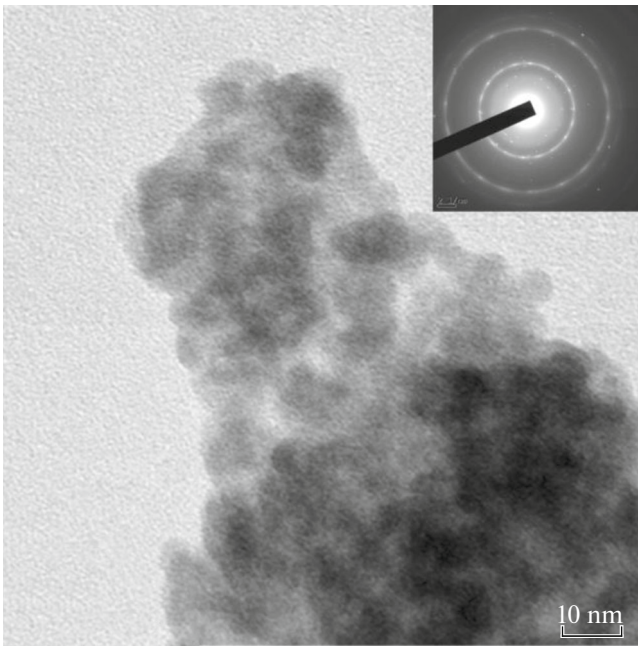

Fig. 5. TEM micrograph and electron diffraction of sample **2** before heat treatment.

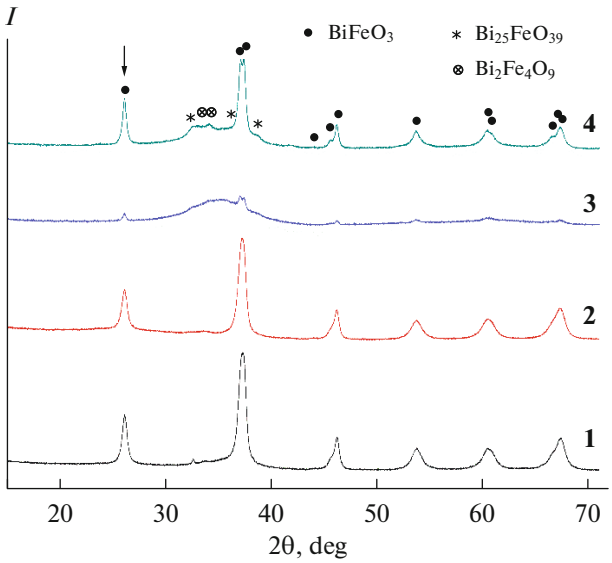

Fig. 6. X-ray diffraction patterns of samples **1**–**4** heat-treated at 490°C for 30 s.

where the symbol "*am*-" points to the amorphous state of the compound, τ_1 and τ_2 are the process duration ($\tau = \tau_1 + \tau_2 = 30$ s).

As can be concluded from the above transformation sequence, the often observed formation of by-products (a phase with the sillenite structure ($Bi_{25}FeO_{39}$), which is enriched in bismuth oxide, and a phase with a mullite structure ($Bi_2Fe_4O_9$), which is enriched in iron oxide compared to $BiFeO_3$) can be due to a local compositional inhomogeneity of the coprecipitated hydroxides. The spatial compositional heterogeneity of the hydroxide mixture can lead to an even greater compositional heterogeneity of the mixture of oxides obtained after dehydration, for the following reason: iron hydroxide dehydrates to form an oxide phase at a lower temperature, i.e., before bismuth hydroxide starts to dehydrate [23], and this would lead to an even greater segregation of phases enriched in bismuth and iron.

The spatial compositional inhomogeneity of an amorphous mixture of bismuth and iron oxides can, in turn, lead to the formation of impurity phases, in the case at hand, phases with the sillenite ($Bi_{25}FeO_{39}$) and mullite ($Bi_2Fe_4O_9$) structures, and to slowing down of $BiFeO_3$ crystallization due to increasing length of the mass transfer of components to the forming $BiFeO_3$ crystalline particles. In this case, the dehydration of mixed amorphous hydroxides can be appreciably extended over temperature and time, and lead to the intermediate formation of a mixture of various phases, the ratio between which will change depending on the temperature and the duration of the process:

$$\begin{aligned} &am\text{-}(Bi_2O_3, Fe_2O_3)\cdot nH_2O \\ &\xrightarrow{-H_2O,\ T} Aam\text{-}(Bi_2O_3, Fe_2O_3)\cdot n'H_2O \\ &+\ Bam\text{-}(Bi_2O_3, Fe_2O_3) + CBi_{25}FeO_{39} \\ &+\ D\ Bi_2Fe_4O_9 + E\ BiFeO_3 \xrightarrow{T,\ \tau} BiFeO_3, \end{aligned} \qquad (2)$$

where A, B, C, D, and E are coefficients showing the ratio of the formed components and depending on the temperature and the duration of the process.

Apparently, a manifestation of some spatial inhomogeneity is a noticeable fraction of the amorphous phase and trace amounts of impurities of crystalline phases ($Bi_2Fe_4O_9$ and $Bi_{25}FeO_{39}$) in samples **3** and **4** as shown by X-ray diffraction (Fig. 6). Thus, it can be concluded that, in order for a mixture of hydroxides to rapidly dehydrate and transform to crystalline bismuth orthoferrite, a bismuth and iron hydroxide mixture must be formed in submerged-jets and free impinging-jets microreactors. The use of these devices intensifies the microscale mixing of reagents [23, 31, 38, 39], thereby making it possible to form hydroxide mixtures upon the hydrolysis of bismuth and iron salts without noticeable spatial separation.

Figure 7 shows the spatial size distribution of $BiFeO_3$ crystallites for samples **1**–**4**, determined from

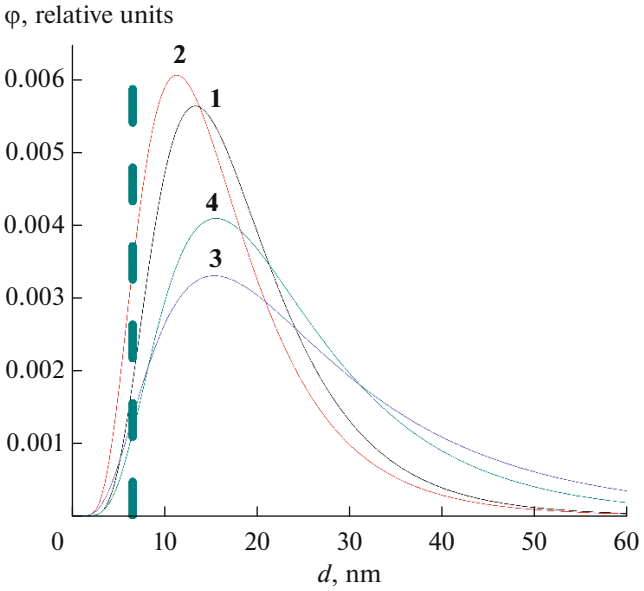

Fig. 7. Spatial crystallite-size distribution for samples **1**–**4** as determined for reflection (012). The dashed line shows the region of the smallest $BiFeO_3$ nanocrystal sizes.

the (012) reflection, which is marked with an arrow in Fig. 6. For samples **1** and **2**, which were prepared in submerged-jets and free impinging-jets microreactors, a narrower crystallite size distribution is observed than for samples **3** and **4**, which were prepared by reverse precipitation without or with ultrasonic treatment.

The weighted-average $BiFeO_3$ crystallite sizes and their root-mean-square deviations according to the crystallite size distribution (Fig. 7) determined for the (012) reflection, are 19 ± 9 nm for sample **1**, 17 ± 9 nm for sample **2**, 28 ± 21 nm for sample **3**, and 24 ± 14 nm for sample **4**.

The following should be mentioned: a wider crystallite-size distribution and the presence of a significant fraction of the amorphous phase and trace amounts of the impurity crystalline phase in samples **3** and **4** (which were prepared with less intensive mixing of the reagents) after heat treatment, indicate that, in this case, the phase formation proceeded according to scheme (2), in contrast to the synthesis of samples **1** and **2**, where scheme (1) involving the rapid formation of $BiFeO_3$ nanocrystals is implemented.

The spatial segregation of the nascent particles of a mixture of hydroxides, the size of which varies within rather narrow bounds (~8–20 nm), is likely to play, too, an essential role in the formation of $BiFeO_3$ nanocrystals with a narrow size distribution when a mixture of bismuth and iron hydroxides is coprecipitated from a mixture of hydroxides (Fig. 5). The possibility of spatial segregation of particles formed when the reagent solutions are reacted under microreactor mixing conditions was shown by the example of the syn-

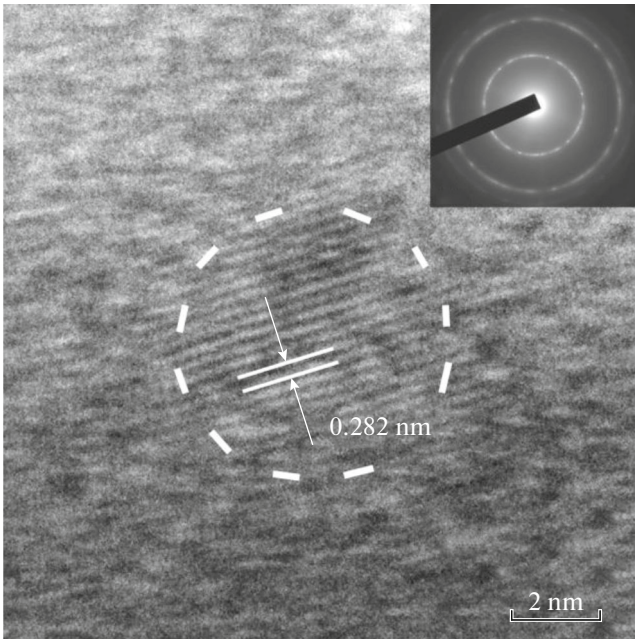

Fig. 8. TEM micrograph of sample **4** after heat treatment.

thesis of various complex oxide phases [23, 31, 40]; this possibility is associated with the specifics of the collision hydrodynamics of liquids, generating Kolmogorov's scale vortices, which manifest themselves as self-organizing nanoreactors. The dehydration of bismuth and iron hydroxide particles of the above sizes will lead to the formation of oxide nanocrystals sized ~7–18 nm if no rapid crystallite growth occurs during the considered period of heat treatment (~30 s), for example, by the oriented growth mechanism [41]. This inference correlates with the experimental results shown in Fig. 7.

Transmission electron microscopy (Fig. 8) showed that discrete bismuth ferrite single crystals sized about 6–7 nm, surrounded by an amorphous phase, were formed in sample **4**. The distance between atomic planes in the crystallite is 0.282 nm (Fig. 8), which corresponds to plane (104) for $BiFeO_3$ (0.2818 nm according to PDF 01-070-5668).

We should mention that the smallest $BiFeO_3$ crystallite sizes as probed by TEM are 6–7 nm both for the crystallites prepared by methods (1) and (2), which provide intensive mixing of the reagents [23, 31, 39, 40], and for the less intensive mixing of reagents (Fig. 7). Since in all these cases $BiFeO_3$ crystals were formed in a very short time via the crystallization of an amorphous phase of the same composition at the same temperature, these crystallite sizes can apparently be considered close to the smallest possible sizes of the bismuth orthoferrite-based crystalline phase. This, in turn, can be related both to the limiting minimum number of unit cell translations required for a stable crystal lattice to form [42] and to the formation of a critical nucleus of the bismuth orthoferrite phase. We should mention that these values of the smallest crystallite size (6–7 nm) are in agreement with the relation $D_{min} \approx L_{unit\ cell} N$ ($N = 10–12$) [42].

CONCLUSIONS

The level of components mixing in the production of bismuth and iron hydroxides dramatically increased when reagent solutions (an equimolar mixed bismuth and iron salt solution and aqueous sodium hydroxide) were reacted in microreactors in the submerged-jets mode under the conditions where the reagent solutions were mixed by free impinging jets to form a thin-film reaction zone (the so-called liquid sheet). The thus-prepared hydroxides, when thermally decomposed at 490°C for 30 s, yielded nanocrystalline bismuth orthoferrite with a narrow crystallite size distribution and with the smallest crystallite sizes (~6–7 nm) free of other impurity phases. Reverse precipitation, even when the microreactor technique and ultrasonic treatment were employed, failed to give equal results (a narrow $BiFeO_3$crystallite size distribution and the absence of impurity phases) at the same hydroxide heat-treatment schedules. However, the smallest $BiFeO_3$ crystallite sizes had similar values (~6–7 nm) regardless of the variant used to form bismuth and iron hydroxide mixtures. This allows us to regard these values as approaching the limiting smallest sizes of $BiFeO_3$ crystallites to be formed under the considered temperature conditions in the crystallization of the initial amorphous material. The study showed the decisive impact of reagent solutions mixing in the production of a mixture of bismuth and iron hydroxides on the possibility of synthesizing nanocrystalline bismuth orthoferrite with a narrow crystallite size distribution and free of other admixture phases that are realized in the Bi_2O_3–Fe_2O_3 system.

ACKNOWLEDGMENTS

X-ray diffraction experiments, scanning electron microscopy, and elemental analysis of the samples were performed on facilities of the Engineering Center of the St. Petersburg State Technological Institute (Technical University).

The transmission electron microscopic studies were carried out using the facilities of the Federal Center for Collective Use "Materials Science and Diagnostics in Advanced Technologies" in the Ioffe Physico-Technical Institute.

FUNDING

The work was supported by the Russian Scientific Foundation (project no. 16-13-10252).

CONFLICT OF INTEREST

The authors declare that they have no conflict of interest.

REFERENCES

1. A. K. Zvezdin and A. P. Pyatakov, Phys. Usp. **47**, 416. https://doi.org/10.1070/PU2004v047n04ABEH001752
2. X. Bai, J. Wei, B. Tian, et al., J. Phys. Chem. **120**, 3595. https://doi.org/10.1021/acs.jpcc.5b09945
3. L. Esmaili and A. Gholizadeh, Iranan J. Crystallogr. Mineral. **26**, 1013 (2019). https://doi.org/10.29252/ijcm.26.4.1013
4. G. Catalan and J. F. Scott, Adv. Mater. **21**, 2463 (2009). https://doi.org/10.1002/adma.200802849
5. A. N. Kalinkin and V. M. Skorikov, Russ. J. Inorg. Chem. **55**, 1794 (2010). https://doi.org/10.1134/S0036023610110173
6. A. P. Pyatakov and A. K. Zvezdin, Phys. Usp. **55**, 557.
7. A. V. Egorysheva, T. I. Milenov, O. G. Ellert, et al., Solid State Sci. **40**, 31 (2015). https://doi.org/10.1016/j.solidstatesciences.2014.12.011
8. M. I. Morozov, N. A. Lomanova, and V. V. Gusarov, Russ. J. Gen. Chem. **73**, 1676 (2003). https://doi.org/10.1023/B:RUGC.0000018640.30953.70
9. J. Silva, A. Reyes, H. Esparza, et al., Integr. Ferroelectr. **126** (1), 47 (2011). https://doi.org/10.1080/10584587.2011.574986
10. V. M. Denisov, N. V. Belousova, V. P. Zhereb, et al. J. Siberian Federal University **5**, 146 (2012). http://elib.sfu-kras.ru/handle/2311/3093.
11. I. Sosnowska, T. P. Neumaier, and E. Streichele, J. Phys. C: Solid State Phys. **15**, 4835 (1982). https://doi.org/10.1088/0022-3719/15/23/020
12. N. A. Lomanova, M. V. Tomkovich, A. V. Osipov, et al., Phys. Solid State **61**, 2535 (2019). https://doi.org/10.1134/S1063783419120278
13. R. Patel and P. Sawadh, Nanosyst.: Phys. Chem. Mater. **10**, 255. https://doi.org/10.17586/2220-8054-2019-10-3-255-265
14. F. Bai, J. Wang, M. Wuttig, et al., Appl. Phys. Lett. **86**, 032511 (2005). https://doi.org/10.1063/1.1851612
15. N. Sheoran, M. Saini, A. Kumar, et al., MRS Adv. **4**, 1659 (2019). https://doi.org/10.1557/adv.2019.167
16. N. A. Lomanova, V. V. Panchuk, V. G. Semenov, et al., Ferroelectrics, 569 (2020).
17. S. M. Selbach, M.-A. Einarsrud, and T. Grande, Chem. Mater. **21**, 169 (2009). https://doi.org/10.1021/cm802607p
18. N. A. Lomanova and V. V. Gusarov, http://nanojournal.ifmo.ru/en/wp-content/uploads/2013/10/NPCM_45P696.pdf.
19. N. A. Lomanova and V. V. Gusarov, Russ. J. Gen. Chem. **83**, 2251 (2013). https://doi.org/10.1134/S1070363213120049
20. A. V. Egorysheva, O. M. Gaitko, P. O. Rudnev, et al., Russ. J. Inorg. Chem. **60**, 1304 (2015). https://doi.org/10.1134/S0036023615110042
21. O. V. Proskurina, M. V. Tomkovich, A. K. Bachina, et al., Russ. J. Gen. Chem. **87**, 2507 (2017). https://doi.org/10.1134/S1070363217110019
22. J.-L. Ortiz-Quiñonez, U. Pal, and M. S. Villanueva, Inorg. Chem. **57**, 6152 (2018). https://doi.org/10.1021/acs.inorgchem.8b00755
23. O. V. Proskurina, I. V. Nogovitsin, T. S. Il'ina, et al., Russ. J. Gen. Chem. **88**, 2139 (2018). https://doi.org/10.1134/S1070363218100183
24. E. Gil-González, A. Perejón, P. E. Sánchez-Jiménez, et al., J. Mater. Chem. A **6** (13), 5356 (2018). https://doi.org/10.1039/C7TA09239C
25. N. A. Lomanova, M. V. Tomkovich, V. V. Sokolov, and V. V. Gusarov, Russ. J. Gen. Chem. **86**, 2256 (2016). https://doi.org/10.1134/S1070363216100030
26. J. Peñalva and A. Lazo, IOP Conf. Series: J. Phys.: Conf. Ser. **1143**, 012025 (2018). https://doi.org/10.1088/1742-6596/1143/1/012025
27. N. A. Lomanova, M. V. Tomkovich, V. V. Sokolov, et al., J. Nanopart. Res. **20**, 17 (2018). https://doi.org/10.1007/s11051-018-4125-6
28. S. Ghosh, S. Dasgupta, A. Sen, and H. S. Maiti, J. Am. Ceram. Soc. **88**, 1349 (2005). https://doi.org/10.1111/j.1551-2916.2005.00306.x
29. A. V. Egorysheva, T. B. Kuvshinova, V. D. Volodin, et al., Inorg. Mater. **49**, 310 (2013). https://doi.org/10.1134/S0020168513030035
30. X. Sun, Z. Liu, H. Yu, et al., Mater. Lett. **219**, 225 (2018). https://doi.org/10.1016/j.matlet.2018.02.052
31. O. V. Proskurina, R. S. Abiev, D. P. Danilovich, et al., Chem. Eng. Process **143**, 107598 (2019). https://doi.org/10.1016/j.cep.2019.107598
32. E. V. Vladimirova, A. V. Dmitriev, and M. V. Kandaurov, Russ. J. Inorg. Chem. **64**, 689 (2019). https://doi.org/10.1134/S0036023619060160
33. S. M. Selbach, T. Tybell, M. A. Einarsrud, and T. Grande, Chem. Mater. **19**, 6478 (2007). https://doi.org/10.1021/cm071827w
34. V. I. Popkov, O. V. Almjasheva, A. S. Semenova, et al., J. Mater. Sci.: Mater. Electron. **28**, 7163 (2017). https://doi.org/10.1007/s10854-017-6676-1
35. V. V. Gusarov, Russ. J. Gen. Chem. **67**, 1846 (1997).
36. M. Missaoui, S. Coste, M. Barré, et al., Nanomaterials **10** (1), 26 (2020). https://doi.org/10.3390/nano10010026
37. A. V. Egorysheva, V. D. Volodin, O. G. Ellert, et al., Inorg. Mater. **49**, 303 (2013). https://doi.org/10.1134/S0020168513030023
38. C. P. Fonte, M. A. Sultan, R. J. Santos, et al., Chem. Eng. J. **260**, 316 (2015). https://doi.org/10.1016/j.cej.2014.08.090
39. R. S. Abiev, Theoret. Found. Chem. Eng. **54** (6) (2020).
40. O. V. Proskurina, E. V. Sivtsov, M. O. Enikeeva, et al., Nanosyst.: Phys. Chem. Mater. **10**, 206 (2019). https://doi.org/10.17586/2220-8054-2019-10-2-206-214
41. V. K. Ivanov, P. P. Fedorov, A. Y. Baranchikov, and V. V. Osiko, Russ. Chem. Rev. **83**, 1204 (2014). https://doi.org/10.1070/RCR4453
42. O. V. Almyasheva, N. A. Lomanova, V. I. Popkov, et al., Nanosyst.: Phys. Chem. Mater. **10**, 428 (2019). https://doi.org/10.17586/2220-8054-2019-10-4-428-437

Translated by O. Fedorova